SANGAM International Journal of Multidisciplinary Research

Vol. 02, Issue 02, March (2025) E-ISSN: 2584-086X

IN PRESENCE OF POROUS MEDIUM INVESTIGATION OF BOUNDARY CONDITIONS ON COUPLED HEAT AND MASS TRANSFER OVER AN ISOTHERMAL SPHERE

Anjali Mewara[1*], Dr. Shweta Bohra[2]

[1*]School of Basic and Applied Sciences, Sangam University, Bhilwara, anjalimewara2716@gmail.com
[2]School of Basic and Applied Sciences, Sangam University, Bhilwara, shweta.bohra@sangamuniversity.ac.in
[*]Corresponding Author: *anjalimewara2716@gmail.com*

Available online at: www.sijmr.org

Abstract— This investigation analyzed how the Soret & Dufour effects influence convective boundary layer flow in nature around an isothermal sphere embedded in a permeable materials, considering different boundary conditions. We have analyzed two prevalent scenarios that define the temp. and conc. distributions between the wall and the surroundings: (a) a constant wall temperature and concentration; (b) a constant surface heat and mass flux; and (c) boundary conditions for convective heat and mass transfer. To facilitate the analysis, an appropriate similarity transformation is employed to convert Ordinary differential equations are created from the governing partial differential equations., with numerical solutions being computed using the bvp4c technique in MATLAB. This study improves our comprehension of how important parameters, Including the permeability parameter K, buoyancy ratio parameter Nb, Soret number Sr, and Dufour number Du, influence the profiles of velocity, temperature, and concentration. The results are conveyed via graphical displays, and the Included are also the Sherwood number, Nusselt number, and skin friction values.

Keywords*— Uniform heat and mass flux, convective boundary conditions, Soret-Dufour effect, porous medium*

I. INTRODUCTION

In engineering contexts, free convective flow is of significant importance. This phenomenon is relevant in various applications, including nuclear combustion chambers, solid matrix heat exchangers, nuclear reactors, and the cooling passages of turbine blades. Throughout the previous years, substantial attention has been directed towards the examination of natural convective flow across a range of geometrical forms. Numerous researchers, including Miyatake and Fuzii [1], Merkin and Chaudhary [2], Paul et al. [3], and Kawala and Odda [4], have conducted extensive studies on laminar free convective flow involving vertical plates, channels, cylinders, and spheres. The study of laminar convective flow over a sphere under uniform heat flux conditions was conducted earlier by Chiang [5]. Additionally, Huang [6] analyzed the natural convection patterns generated by a sphere, considering the effects of both blowing and suction. Given the relevance of mass transfer in engineering, scientific fields, and industry, Molla et al. [7] The study revealed the effects of chemical reactions on the transfer of heat and mass surrounding an isothermal sphere. Subsequently, Molla et al. [8, 9] reported results concerning heat transfer in natural convective flow from an isothermal sphere, considering heat generation and radiation effects, respectively. Nazar et al. [10, 11] The research investigated. The boundary layer of natural convection flow of micropolar fluids, with a particular emphasis on two specific boundary conditions: constant wall and constant heat flux (CHF) temp. (CWT). Furthermore, Tahmina [12] looked at the role of radiation in free convective flow coming from an isothermal sphere with a constant heat flux. Chamkha et al. [13] numerically calculated the friction factor, mass transfer rate, and surface heat transfer rate in natural convection around an isothermal sphere. Taking into consideration partial slip, the role of a permeable sphere in a porous medium, radiation effects, and heat generation, Gaffar et al. [14,15] investigated the dynamics of heat and mass transfer in the boundary layer flow of a non-Newtonian fluid adjacent to an isothermal sphere.

Taha et al. [16] investigated the magnetohydrodynamic free convection boundary layer flow around a solid sphere using radiation effects and convective boundary conditions. When heat and mass transfer in a moving fluid are examined combined, a complex relationship between the fluxes and the driving potentials is revealed. The energy flux and mass flux, which are produced by concentration and temperature gradients, respectively, impacted by the Soret and Dufour effects, are the source of this complexity. Many academics have investigated these effects in the context of natural convective flow under a variety of settings, notably Dursurkaya [17]–[22].

Numerous studies have focused on heat and mass transfer in situations where there is a constant flow of heat. For example, Srinivas acharya and Mendu [23] investigated how mixed convective flow along a semi-vertical infinite

plate is affected by varying heat and mass fluxes. Furthermore, taking homogeneous heat, mass, and nanoparticle fluxes into account, Srinivas acharya and Surender [24] examined the Soret-Dufour effects on the flow of a nanofluid over a vertical flat plate in a porous media using a mixed convective boundary layer.

Swarnalathamma [25] investigated the heat and mass transfer characteristics of an Eyring-Powel nanofluid flowing magnetohydrodynamically (MHD) around an isothermal sphere, taking into consideration the effects of thermal slip. A. Subba Rao et al. [26] contributed to this field by simulating the hydromagnetic convection slip flow of a Casson non-Newtonian nanofluid emanating from an isothermal sphere. Subsequently, Sedki [27] explored the influence of thermal radiation and chemical reactions on MHD mixed convective heat and mass transfer in nanofluid flow induced by a nonlinear stretching surface within a porous medium. Finally, Krishna et al. [28] focused on the heat and mass transfer processes in MHD flow of a second-grade fluid over a semi-infinite vertical stretching sheet situated in a porous medium. Dulal et al. [29] conducted a study on the magneto-soret-Dufour thermo-radiative double-diffusive convection heat and mass transfer of a micropolar fluid within a porous medium, incorporating factors such as ohmic dissipation and variable thermal conductivity. In a related investigation, Amir et al. [30] examined the influence of radiative heat transfer and reduced gravity on magnetohydrodynamic (MHD) flow around a stationary, non-rotating sphere situated in a porous medium. Keshavarzian et al. [31] explored the validity of the local thermal equilibrium assumption in the context of free convection boundary layer flow over a horizontal cylinder submerged in an infinite saturated porous material. Their results revealed that the average temperature difference between the fluid and solid could increase by 200% as the Prandtl number escalated from 2 to 7, while a rise in the Bio number from 0.01 to 10 could lead to a 33% decrease. Additionally, the temperature difference could increase sevenfold with porosity rising from 0.25 to 0.85, and by 50% as the ratio of cylinder to particle diameter expanded from 20 to 100. Building on Keshavarzian's findings, Hamida et al. [32] performed a numerical analysis aimed at enhancing heat and mass transfer during the drying of building bricks in a porous medium using hybrid nanofluids. Their results indicated that the water-Al2O3-MgO hybrid nanofluid exhibited significantly poorer heat and mass transfer characteristics compared to pure water and the water-Al2O3-SiO2 mixture. They also noted a reduction in drying time for the second phase as the surrounding temperature increased.

Francis et al. [33] conducted a computational analysis of bio-convective Eyring Powell nanofluid flow influenced by magneto-hydrodynamic consequences over an isothermal cone surface with a convective boundary condition. Their findings indicate that a hike in the volume fraction ($0.01 \leq \varphi \leq 0.03$) results in enhancements of mass and heat transfer by 3% and 3.5%, respectively. Additionally, they observed that soar in the magneto-hydrodynamic parameter ($1 \leq M \leq 3$), porosity ($1 \leq \Gamma \leq 3$), and the Eyring-Powell fluid parameter ($0 \leq K \leq 0.3$) leads to a reduction in velocity by as much as 23%, while simultaneously improving heat, mass transfer, and microorganism diffusion rates.

Furthermore, an increase in the Joule heating parameter ($1 \leq Ju \leq 3$) contributes to a 21% enhancement in heat transfer. Lastly, an hike in the viscous dissipation parameter ($0.3 \leq Ec \leq 0.9$) results in a boost in mass and heat transfer by 6% and 8%, respectively. Khan W. et al. [34] explored two-dimensional steady squeezing flow within A porous channel that is vertical, with an focus on free convective heat and mass transfer under constant suction. They examined the effects of the Soret & Dufour parameters on heat from natural convection and mass transport in a two-dimensional boundary layer flow. They discovered that suction produced two solution branches, and the stability of these branches was confirmed by eigen value analysis.

This study demonstrates how numerous parameters have a substantial impact on flow characteristics and how beneficial they are for chemical engineering applications. In this study, we investigate the Soret and Dufour effects on natural convective flow around an isothermal sphere in a porous material while taking into account three different boundary conditions.: 1) constant mass flux and heat, 2) constant wall temperature and concentration, and 3) convective boundary conditions.

II. MATHEMATICAL FORMULATION

An isothermal-sphere of radius 'a' is analysed while being situated within a porous media. This sphere is heated to a temperature denoted as T_w, with a corresponding heat flux q_w and concentration C_w, along with a mass flux q_m. The temperature and concentration of the surrounding environment are represented as C_∞ . The surface concentration C_w and temperature T_w are sustained through Heat transfer by convection at specific values of T_f and C_f, respectively. In the defined coordinate system, the x-coordinate measures along the sphere's surface from its lowest point, while the y-coordinate is inclinable normal to the surface. The velocity components are represented by u and v , corresponding to the x and y directions, respectively. The physical model and coordinate system are illustrated in Fig. 1. The radial distance between the sphere's surface and the axis of symmetry is indicated as $r = a \sin\left(\frac{x}{a}\right)$.

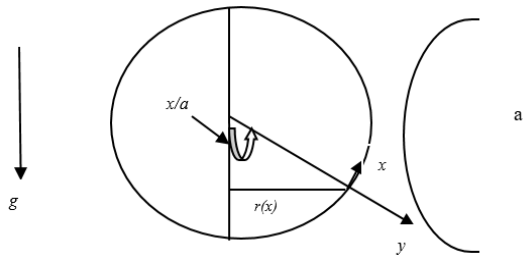

Fig. 1. Physical diagram of the problem

Let the fluid temperature and concentration be denoted as T and C, respectively, while T_m represents the mean fluid temperature. The fluid possesses kinematic viscosity $\nu = \frac{\mu}{\rho}$ and density ρ. The parameters for thermal diffusivity, mass diffusivity, and thermal conductivity are represented as $\alpha = \frac{k}{\rho C_p}$, D_m, and k, respectively. The variable g signifies the acceleration because of gravity, while β and β^* denote the coefficients of thermal expansion & concentration expansion, respectively. specific heat capacity C_P, the thermal diffusion ratio is K_T, the concentration susceptibility denoted by C_s, and k_0 represents the permeability coefficient. The governing equations are founded by using the Oberbeck–Boussinesq approximation. The following are the mass, momentum, energy, and concentration conservation equations under these assumptions and the conventional boundary layer approximations:

$$\frac{\partial}{\partial x}(ru) + \frac{\partial}{\partial y}(rv) = 0 \tag{1}$$

$$u\frac{\partial u}{\partial x} + v\frac{\partial u}{\partial y} = \nu\frac{\partial^2 u}{\partial y^2} + g\beta(T - T_\infty)\,sin\left(\frac{x}{a}\right) + g\beta^*(C - C_\infty)\,sin\left(\frac{x}{a}\right) - \frac{\nu u}{k_0} \tag{2}$$

$$u\frac{\partial T}{\partial x} + v\frac{\partial T}{\partial y} = \alpha\frac{\partial^2 T}{\partial y^2} + \frac{D_m K_T}{C_s C_P}\frac{\partial^2 C}{\partial y^2} \tag{3}$$

$$u\frac{\partial C}{\partial x} + v\frac{\partial C}{\partial y} = D_m\frac{\partial^2 C}{\partial y^2} + \frac{D_m K_T}{T_m}\frac{\partial^2 T}{\partial y^2} \tag{4}$$

The resolution of the aforementioned equations is examined and evaluated in the context of three distinct boundary conditions. Which we divide in three cases:

Case 1- At a relatively stable concentration and wall temperature

Boundary conditions in this instance are understood to be:

at $y = 0$ $\{u = v = 0, \quad T = T_w, C = C_w\}$

at $y \to \infty$ $\{u \to 0, \quad T \to T_\infty, \quad C \to C_\infty\}$ (5)

For this case, introducing similarity transformation

$$\xi = \frac{x}{a}, \quad \eta = \frac{y}{a}Gr^{\frac{1}{5}}, \quad \psi = r\nu\xi f(\xi,\eta)Gr^{\frac{1}{5}}, \quad Gr = \frac{g\beta(T_w - T_\infty)a^3}{\nu^2},$$

$$\theta(\xi,\eta) = \frac{T - T_\infty}{T_w - T_\infty}, \quad \phi(\xi,\eta) = \frac{C - C_\infty}{C_w - C_\infty} \tag{6}$$

Where, thermal Grashof number represent by Gr and ψ is stream function which is shows by

$$u = \frac{1}{r}\frac{\partial \psi}{\partial y} = \frac{\nu Gr^{\frac{2}{5}}}{a}\xi f' \quad \text{and}$$

$$v = -\frac{1}{r}\frac{\partial \psi}{\partial x} = \frac{-\nu Gr^{\frac{1}{5}}}{a}\left[\xi\frac{\partial f}{\partial \xi} + f + f\xi\,cot\,\xi\right] \tag{7}$$

Substituting equations (6)-(7) in equations (1)-(4) and obtained non dimensional ordinary differential equations:

$$f''' + (1 + \xi\,cot\,\xi)ff'' - f'^2 + \frac{sin\xi}{\xi}(\theta + N_b\phi) - \frac{1}{K}f' = \xi\left(f'\frac{\partial f_\prime}{\partial \xi} - f''\frac{\partial f}{\partial \xi}\right), \tag{8}$$

$$\theta'' + Pr(1 + \xi\,cot\,\xi)f\theta' + Pr\,D\,u\phi'' = Pr\,\xi\left(f'\frac{\partial \theta}{\partial \xi} - \frac{\partial f}{\partial \xi}\theta'\right), \tag{9}$$

$$\phi'' + Sc(1 + \xi\,cot\,\xi)f\phi' + ScSr\theta'' = Sc\xi\left(f'\frac{\partial \phi}{\partial \xi} - \frac{\partial f}{\partial \xi}\phi'\right), \tag{10}$$

Subjected to boundary conditions

$$\text{At } \eta = 0 \begin{cases} f(\xi,0) = 0, \\ f'^{(\xi,0)} = 0, \\ \theta(\xi,0) = 1, \\ \phi(\xi,0) = 1 \end{cases} \text{ at } \eta \to \infty \begin{cases} f'^{(\xi,0)} \to 0, \\ \theta(\xi,0) \to 0, \\ \phi(\xi,0) \to 0, \end{cases} \tag{11}$$

where ξ is the dimensionless tangential coordinate, and the differentiation with respect to η is shown by the primes., the radial coordinate without dimensions.

$K = \frac{k_0 Gr^{\frac{2}{5}}}{a^2}$ is permeability parameter, Prandtl number is $Pr = \frac{\nu}{\alpha}$, Schmidt number denoted by $Sc = \frac{\nu}{D_m}$. $N_b = \frac{\beta^*(C_w - C_\infty)}{\beta(T_w - T_\infty)}$ is parameter of ratio of concentration to thermal buoyancy. $Du = \frac{D_m K_T (C_w - C_\infty)}{\nu C_s C_P (T_w - T_\infty)}$ and $Sr = \frac{D_m K_T (T_w - T_\infty)}{\nu T_m (C_w - C_\infty)}$ are Dufour & Soret number respectively.

Case 2- At a relatively stable heat and mass flux

In subject boundary conditions are taken as:

$$\text{at} \quad y = 0 \{u = v = 0, \quad q_w = -k\left(\frac{\partial T}{\partial y}\right), \quad q_m = -D_m\left(\frac{\partial C}{\partial y}\right)\}$$

$$\text{at} \quad y \to \infty \{u \to 0, \quad T \to T_\infty, \quad C \to C_\infty\} \tag{12}$$

Introducing similarity transformation

$$\xi = \frac{x}{a}, \quad \eta = \frac{y}{a} Gr^{\frac{1}{5}}, \quad \psi = r\nu\xi f(\xi,\eta) Gr^{\frac{1}{5}}, \quad Gr = g\beta\left(\frac{q_w}{k}\right)\frac{a^4}{\nu^2}$$

$$\theta(\xi,\eta) = \frac{T - T_\infty}{a\frac{q_w}{k}} Gr^{\frac{1}{5}}, \quad \phi(\xi,\eta) = \frac{C - C_\infty}{a\frac{q_m}{D_m}} Gr^{\frac{1}{5}} \tag{13}$$

Where, Gr is thermal Grashof number and the stream function ψ is defined by

$$u = \frac{1}{r}\frac{\partial \psi}{\partial y} = \frac{\nu Gr^{\frac{2}{5}}}{a}\xi f' \qquad \text{and}$$

$$v = -\frac{1}{r}\frac{\partial \psi}{\partial x} = \frac{-\nu Gr^{\frac{1}{5}}}{a}\left[\xi\frac{\partial f}{\partial \xi} + f + f\xi\cot\xi\right] \tag{14}$$

Substituting equations (13)-(14) in equations (1)-(4) and obtained non-dimensional ordinary differential equations:

$$f''' + (1 + \xi\cot\xi)ff'' - f'^2 + \frac{\sin\xi}{\xi}(\theta + N_b\phi) - \frac{1}{K}f' = \xi\left(f'\frac{\partial f'}{\partial \xi} - f''\frac{\partial f}{\partial \xi}\right), \tag{15}$$

$$\theta'' + Pr(1 + \xi\cot\xi)f\theta' + Pr\,D\,u\phi'' = Pr\,\xi\left(f'\frac{\partial \theta}{\partial \xi} - \frac{\partial f}{\partial \xi}\theta'\right), \tag{16}$$

$$\phi'' + Sc(1 + \xi\cot\xi)f\phi' + ScSr\theta'' = Sc\xi\left(f'\frac{\partial \phi}{\partial \xi} - \frac{\partial f}{\partial \xi}\phi'\right), \tag{17}$$

Subject to boundary conditions

$$\text{at} \quad \eta = 0 \begin{cases} f(\xi,0) = 0, \\ f'(\xi,0) = 0, \\ \theta'^{(\xi,0)} = -1 \\ \phi'(\xi,0) = -1 \end{cases} \quad \text{and} \quad \eta \to \infty \begin{cases} f'^{(\xi,0)} \to 0, \\ \theta(\xi,0) \to 0 \\ \phi(\xi,0) \to 0, \end{cases} \tag{18}$$

where ξ is the dimensionless tangential coordinate, and the differentiation with respect to η is shown by the primes., the radial coordinate without dimensions.

$K = \frac{k_0 Gr^{\frac{2}{5}}}{a^2}$ is permeability parameter, $Pr = \frac{\nu}{\alpha}$ is Prandtl number, $Sc = \frac{\nu}{D_m}$ is Schmidt number.

$N_b = \frac{\beta^* q_m k}{\beta q_w D_m}$ is parameter for the concentration to thermal buoyancy ratio, $Du = \frac{D_m K_T q_m k}{\nu C_s C_P D_m q_w}$ and $Sr = \frac{K_T q_w}{\nu T_m q_m k}$ are Dufour and Soret number respectively.

Case 3- At relatively stable boundary conditions

Under convective boundary conditions, the mass transfer coefficient km and heat transfer coefficient hf are given as

$$\text{at} \quad y = 0 \ \{u = v = 0, \quad -k\frac{\partial T}{\partial y} = h_f(T_f - T), -D_m\frac{\partial C}{\partial y} = k_m(C_f - C)\}$$

$$\text{at} \ \ y \to \infty \{u \to 0, \quad T \to T_\infty, \quad C \to C_\infty\} \tag{19}$$

Introducing similarity transformation

$$\xi = \frac{x}{a}, \quad \eta = \frac{y}{a}Gr^{\frac{1}{5}}, \quad \psi = r\nu\xi f(\xi,\eta)Gr^{\frac{1}{5}}, \quad Gr = \frac{g\beta(T_f - T_\infty)a^3}{\nu^2},$$

$$\theta(\xi,\eta) = \frac{T - T_\infty}{T_f - T_\infty}, \ \phi(\xi,\eta) = \frac{C - C_\infty}{C_f - C_\infty} \tag{20}$$

Where, thermal Grashof number is Gr and the stream function is ψ.

$$u = \frac{1}{r}\frac{\partial \psi}{\partial y} = \frac{\nu Gr^{\frac{2}{5}}}{a}\xi f' \qquad \text{and}$$

$$v = -\frac{1}{r}\frac{\partial \psi}{\partial x} = \frac{-\nu Gr^{\frac{1}{5}}}{a}\left[\xi\frac{\partial f}{\partial \xi} + f + f\xi\cot\xi\right] \tag{21}$$

Substituting equations (20)-(21) in equations (1)-(4) and obtained non-dimensional ordinary differential equations:

$$f''' + (1 + \xi\cot\xi)ff'' - f'^2 + \frac{\sin\xi}{\xi}(\theta + N_b\phi) - \frac{1}{K}f' = \xi\left(f'\frac{\partial f'}{\partial \xi} - f''\frac{\partial f}{\partial \xi}\right), \tag{22}$$

$$\theta'' + Pr(1 + \xi\cot\xi)f\theta' + Pr\,D\,u\phi'' = Pr\,\xi\left(f'\frac{\partial \theta}{\partial \xi} - \frac{\partial f}{\partial \xi}\theta'\right), \tag{23}$$

$$\phi'' + Sc(1 + \xi\cot\xi)f\phi' + ScSr\theta'' = Sc\xi\left(f'\frac{\partial \phi}{\partial \xi} - \frac{\partial f}{\partial \xi}\phi'\right), \tag{24}$$

Subject to boundary conditions

$$\text{at} \quad \eta = 0 \begin{cases} f(\xi,0) = 0, \\ f'^{(\xi,0)} = 0, \\ \theta'^{(\xi,0)} = -Bi_1(1 - \theta), \\ \phi'(\xi,0) = -Bi_2(1 - \phi) \end{cases} \quad \text{at} \quad \eta \to \infty \begin{cases} f'^{(\xi,0)} \to 0 \\ \theta(\xi,0) \to 0 \\ \phi(\xi,0) \to 0 \end{cases} \tag{25}$$

where ξ is the dimensionless tangential coordinate, and the differentiation with respect to is shown by the primes, the dimensionless radial coordinate.

thermal Biot number $Bi_1 = \frac{ah_f Gr^{-1/5}}{k}$ and $Bi_2 = \frac{ak_m Gr^{-1/5}}{D_m}$ is concentration Biot number,

$K = \frac{k_0 Gr^{\frac{2}{5}}}{a^2}$ is permeability parameter, $Pr = \frac{\nu}{\alpha}$ is The physical property of the Prandtl number, or Pr, is that it compares momentum and thermal diffusion. For air and water, respectively, Pr is assumed to be 0.71 and 7.0.

$Sc = \frac{\nu}{D_m}$ is Schmidt number. Sc stands for the mass diffusivity to momentum ratio. Schmidt number values are calculated as follows: Sc = 0.22, 0.66, 0.94, 1, 2, 2.62 for hydrogen, oxygen, carbon dioxide, methanol, ethyl benzene, and propyl benzene, respectively. These values correspond to airborne spreading chemical species of most interest.

$N_b = \frac{\beta^*(C_f - C_\infty)}{\beta(T_f - T_\infty)}$ is the parameter for the ratio of concentration to thermal buoyancy. Nb=1 shows that the thermal and species buoyancy forces are of the same order of magnitude and reinforce each other.

$Du = \frac{D_m K_T (C_f - C_\infty)}{\nu C_s C_P (T_f - T_\infty)}$ and $Sr = \frac{D_m K_T (T_f - T_\infty)}{\nu T_m (C_f - C_\infty)}$ are Dufour and Soret number respectively.

Whereas the Soret number shows how temperature gradients affect the diffusion of mass (species), the Dufour number shows how concentration gradients affect thermal energy transfer within a flow. In combinations with light molecular weights, such as hydrogen and air (H_2), the Soret and Dufour effects are very significant. For example, the Soret effect has been effectively applied to the isotope separation process and to mixes of gases with very light molecular weights, such as hydrogen and helium (He,H_2), and medium molecular weights, such as nitrogen and air (N_2). Recent studies have shown that the Dufour effect can also have a big effect.

The normalized surface shear stress function, or skin friction coefficient Cf, is as follows for each of the three scenarios:

$$C_f = \frac{\tau_w}{\rho U_\infty^2},$$

For natural convection $\rho U_\infty^2 \square\ ag\Delta\rho, \quad U_\infty^2 = \frac{ag\Delta\rho}{\rho} = \frac{a^3 g(\Delta\rho/\rho)}{\nu^2}\left(\frac{\nu^2}{a^2}\right) = Gr\left(\frac{\nu^2}{a^2}\right)$

$C_f = \frac{\tau_w a^2}{\rho \nu^2 Gr}$, Here $\tau_w = \mu\left(\frac{\partial u}{\partial y}\right)_{y=0} = \frac{\mu \nu Gr^{3/5}}{a^2}\xi f''(\xi, 0),$

Therefore, $Gr^{2/5} C_f = \xi f''(\xi, 0).$

rate of dimensionless surface heat transfer **(Nusselt number *Nu*)**:

Case 1-

$$Nu = \frac{a q_w}{k(T_w - T_\infty)},$$

Here, $q_w = -k\left(\frac{\partial T}{\partial y}\right)_{y=0} = \frac{k(T_w - T_\infty) Gr^{1/5}}{a}\left[-\theta'(\xi, 0)\right]$

Therefore, $Gr^{-1/5} Nu = -\theta'(\xi, 0).$

Case 2-

$$Nu = \frac{aq_w}{k\left(T_w - T_\infty\right)}, \qquad \text{Here, } q_w = -k\left(\frac{\partial T}{\partial y}\right)_{y=0}$$

Therefore, $Gr^{-1/5} Nu = \frac{1}{\theta(\xi,0)}.$

Case 3-

$$Nu = \frac{aq_w}{k\left(T_f - T_\infty\right)},$$

Here, $q_w = -k\left(\frac{\partial T}{\partial y}\right)_{y=0} = \frac{k\left(T_f - T_\infty\right)Gr^{1/5}}{a}\left[-\theta'(\xi,0)\right]$

Therefore, $Gr^{-1/5} Nu = -\theta'(\xi,0).$

rate of dimensionless surface heat transfer **(Sherwood number *Sh*)**:

Case 1-

$$Sh = \frac{am_w}{D_m\left(C_w - C_\infty\right)},$$

Here, $m_w = -D_m\left(\frac{\partial C}{\partial y}\right)_{y=0} = \frac{D_m\left(C_w - C_\infty\right)Gr^{1/5}}{a}\left[-\phi'(\xi,0)\right]$

Therefore, $Gr^{-1/5} Sh = -\phi'(\xi,0).$

Case 2-

$$Sh = \frac{am_w}{D_m\left(C_w - C_\infty\right)}, \qquad \text{Here,} \qquad m_w = -D_m\left(\frac{\partial C}{\partial y}\right)_{y=0}$$

Therefore, $Gr^{-1/5} Sh = \frac{1}{\phi(\xi,0)}.$

Case 3-

$$Sh = \frac{am_w}{D_m\left(C_f - C_\infty\right)},$$

Here, $m_w = -D_m\left(\frac{\partial C}{\partial y}\right)_{y=0} = \frac{D_m\left(C_f - C_\infty\right)Gr^{1/5}}{a}\left[-\phi'\left(\xi,0\right)\right]$

Therefore, $Gr^{-1/5}\,Sh = -\phi'\left(\xi,0\right).$

Solution

In the current study, the ODE system is solved numerically using MATLAB's bvp4c approach. We have compared the current results with those of case 1: Huang and Chen [6] and Nazar et al. [10], case 2: Chiang et al. [5] and Molla et al. [8], and case 3: Alkasasbeh et al. [16] under identical physical conditions in order to verify the accuracy of this approach. The results obtained are in good agreement, as shown in Tables 1, 2, and 3.

We set the default values of Pr = 0.71 (air), Sc = 0.22 (for hydrogen at constant temperature 250 C), Sr = 0. 25, Du = 0.2 (product of Sr and Du should be constant), K = 0.5, Nb = 1, $\xi = \frac{\pi}{4}$ until they change, unless the results are displayed in Fig. 2–Fig. 6. This allows us to ascertain how different parameters affect the temperature, velocity, and concentration distributions. Here, we covered the situations of mass and heat transfer at constant concentration and wall temperature as well as constant mass and heat flow for changes in each parameter.

Table 1

Comparison of the current study's findings with those published by Huang and Chen [6] and Nazar *et al.* [10] of the heat transfer coefficient $-\theta'\left(\xi,0\right)$ at the lower stagnation point $\xi \approx 0$ of the sphere

for Pr = 0.7, *Sr* = *Du* = N_b = *Sc* = 0 and $K \to \infty$

Huang and Chen [6]	**Nazar *et al.* [10]**	**Present**
0.4574	0.4576	0.457566777

Table 2

Comparison between the results of present study with the results reported by Chiang *et al.* [5] and Molla *et al.* [8] for surface temperature $\theta(\xi, 0)$ for Pr = 0.71, *Sr* = *Du* = N_b = *Sc* = 0 and $K \to \infty$

	ξ					
	0^0	**20^0**	**30^0**	**45^0**	**60^0**	**90^0**
Chiang et al. (1964)	1.8691	1.8790	1.8913	1.9192	1.9582	2.0696
Molla et al.(2006)	1.8691	1.8797	1.8927	1.9224	1.9660	2.1047
Present	1.8632	1.8799	1.9017	1.9544	2.0393	2.4165

Table 3

Comparison between the results of present study with the results reported by Alkasasbeh *et al.* [16] of the heat transfer coefficient $-\theta'\left(\xi,0\right)$ at the lower stagnation point $\xi \approx 0$ of the sphere for Pr = 0.7, Bi_1 = 0.1, *Sr* = *Du* = N_b = *Sc* = 0, $Bi_2 \to \infty$ and $K \to \infty$

Alkasasbeh et al. [16]	**Present**
0.076195	0.076171162

III. RESULT AND DISCUSSION

1. Effect of permeability parameter *K*-

In Figures 2(a) to 2(c), the influence of K on the profiles of velocity, temperature, and concentration is illustrated. It is evident that as the value of K rises, the velocity also increases, while both temperature and concentration exhibit a decline in both scenarios. This phenomenon occurs because the porosity of the fluid generates a Darcy resistance force within the system, which diminishes as permeability increases. As a result, the flow velocity increases while the temperature and concentration distributions decrease because the Darcy resistance force has less of an impact.

Effect of buoyancy ratio parameter N_b -

Figures 3(a) through 3(c) show how Nb affects the velocity, temperature, and concentration curves. In this analysis, we consider three scenarios: Nb < 0, Nb = 0, and Nb > 0. When Nb = 0, natural convection is solely driven by thermal buoyancy forces, with no influence from species diffusion. Conversely, Nb > 0 indicates that the buoyancy force resulting from species diffusion contributes positively, while Nb < 0 suggests the opposite effect. As depicted in Figure 3(a), it is found that the velocity increases as Nb transitions from a negative to a positive value, whereas the temperature and concentration exhibit an opposite trend.

2. Effect of Soret Sr and Dufour Du number-

The investigation focuses on the combined influence of the Sr-Du number, as illustrated in Figures 4(a) to 4(c). Notably, an hike in the Du value corresponds with a decrease in the Sr value. In Figure 4(a), it is found that the velocity distribution diminishes as the Sr number increases, concurrently with a decrease in Du. Upon examining Figures 4(b) and 4(c), it becomes evident that a reduction in Du (which corresponds to an increase in Sr) leads to a decrease in temperature while simultaneously increasing the fluid concentration. This phenomenon occurs because a lower Du (higher Sr) diminishes the effect of the mass gradient on temperature, thereby enhancing the contribution of the temperature gradient to mass diffusion. Consequently, the boundary layer experiences cooling, resulting in an increased concentration within that regime.

3. Effect of Prandtl number Pr-

The influence of the Pr (Prandtl number) on velocity, temperature, and mass distribution is illustrated in Figures 5(a) to 5(c). It is noticed that a higher Pr value leads to an enhancement of viscous effects, resulting in a thicker viscous boundary layer compared to the thermal boundary layer. Consequently, both velocity and temperature decrease, while the concentration profile exhibits the opposite trend as Pr increases.

4. Effect of Schmidt number Sc-

The effect of the Schmidt number on the velocity, temperature, and concentration profiles in each of the three scenarios is shown in Figures 6(a)–6(c). It was observed that while temperature rises with an increase in Schmidt number, velocity and concentration fall. This pattern is consistent across all three cases examined in our study.

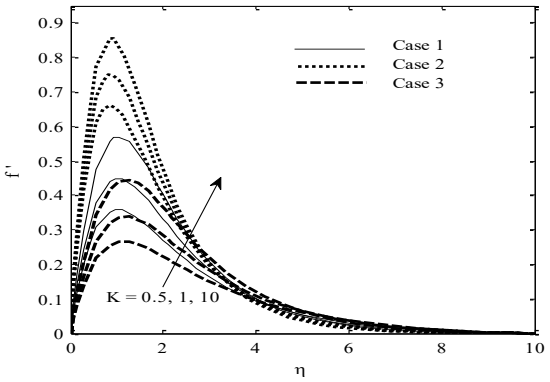

Fig. 2 (a) The velocity profile Effected by K

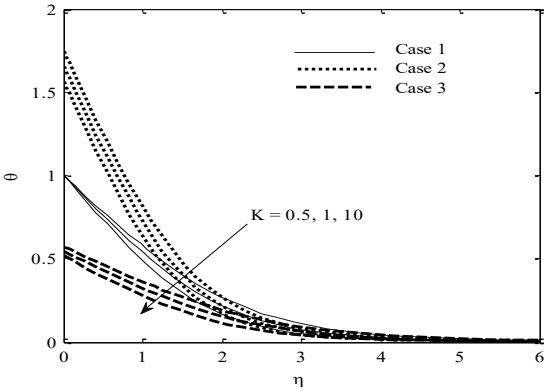

Fig. 2 (b) Temperature profile Effected by K

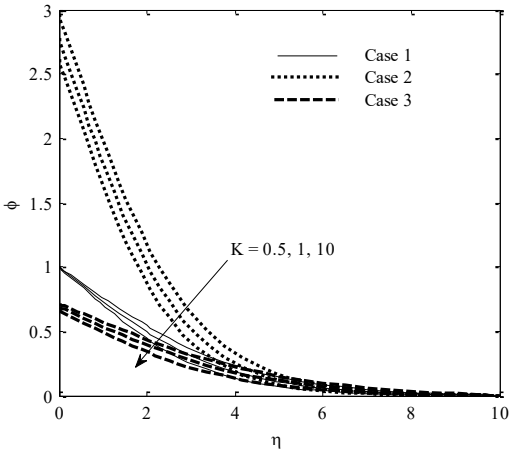

Fig. 2 (c) The concentration profile Effected by K

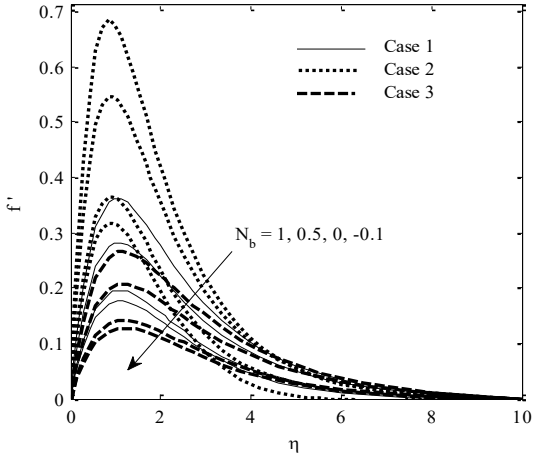

Fig. 3 (a) Velocity profile Effected by N

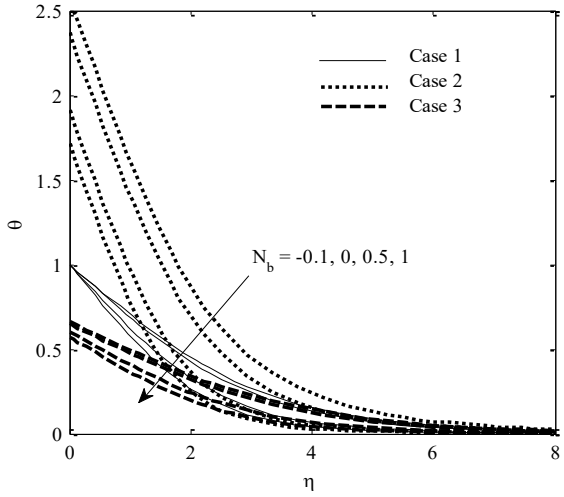

Fig. 3 (b) Temperature profile Effected by N

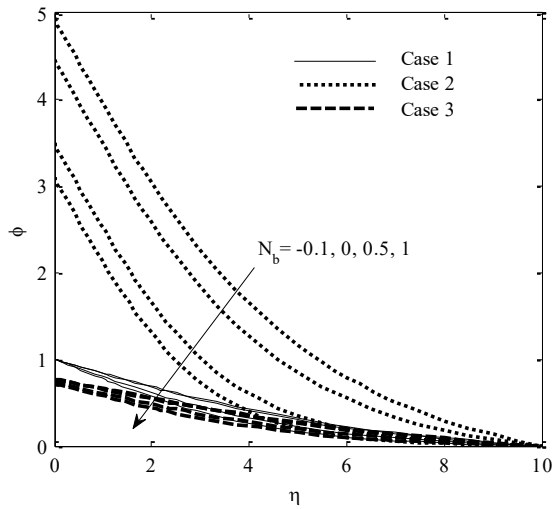

Fig. 3 (c) Concentration profile Effected by N

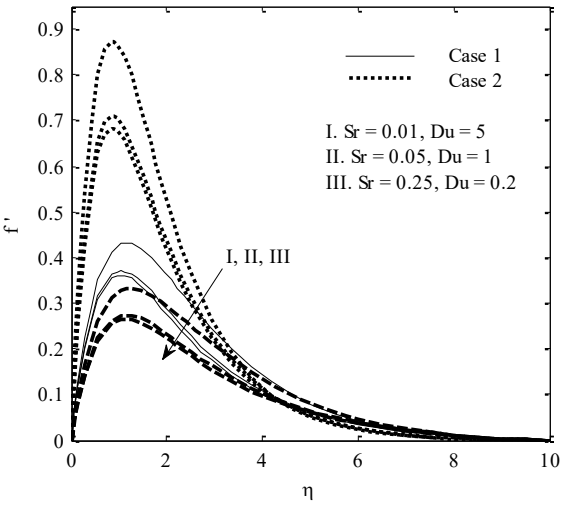

Fig. 4 (a) Velocity profile Effected by Sr-Du

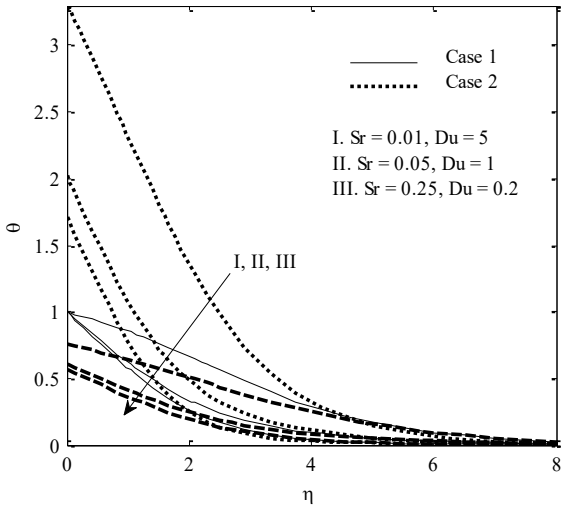

Fig. 4 (b) Temperature profile Effected by Sr-Du

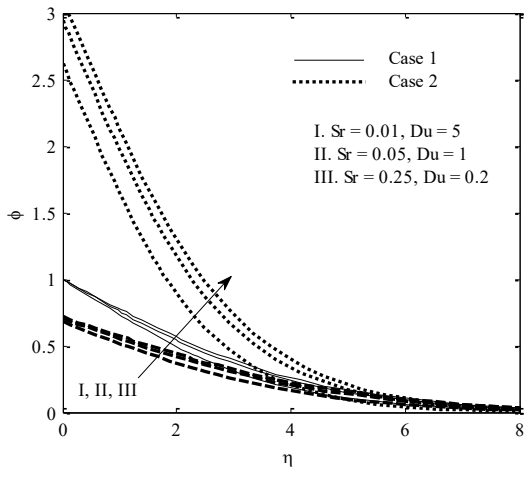

Fig. 4 (c) Concentration profile Effected by Sr-Du

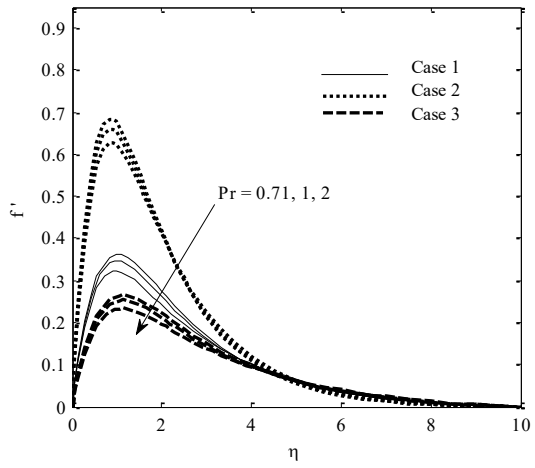

Fig. 5 (a) Velocity profile Effected by Pr

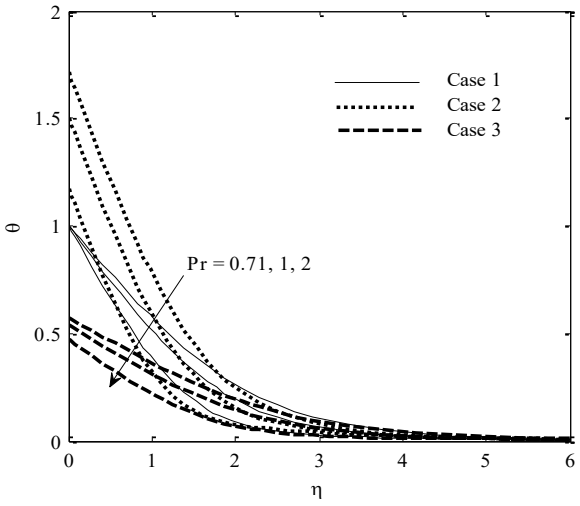

Fig. 5 (b) Temperature profile Effected by Pr

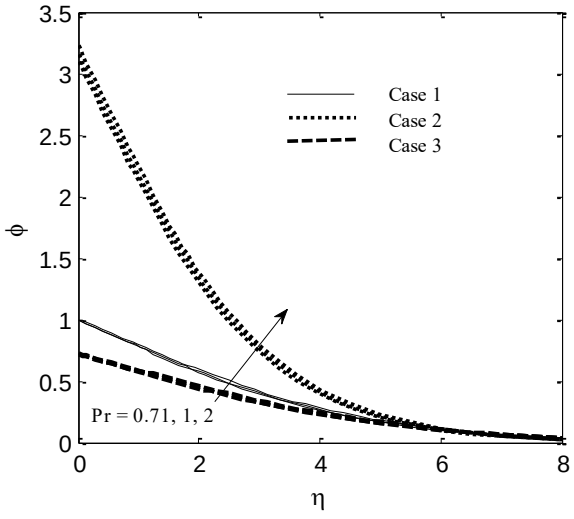

Fig. 5 (c) Concentration profile Effected by Pr

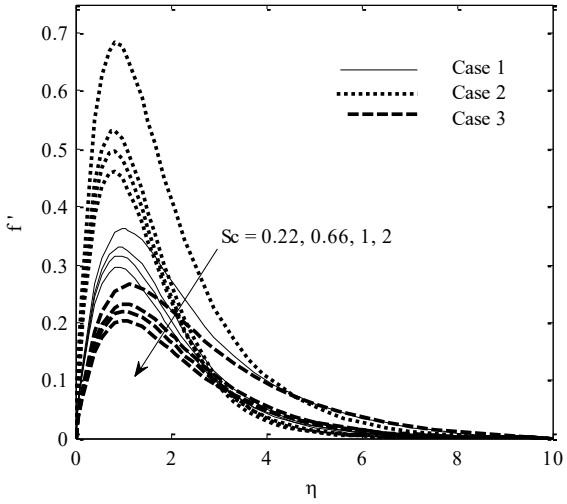

Fig. 6 (a) Velocity profile Effected by Sc

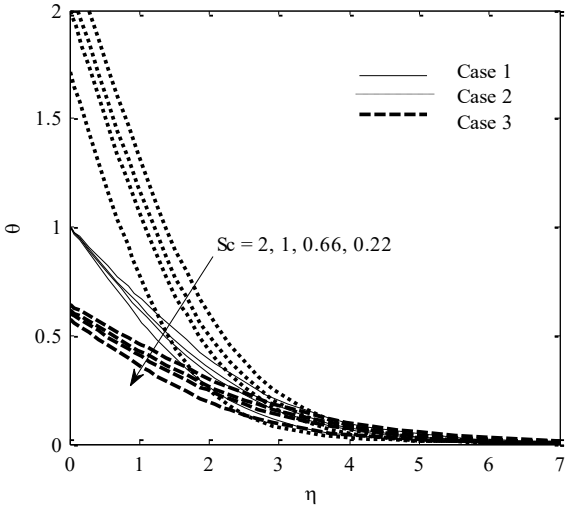

Fig. 6 (b) Temperature profile Effected by Sc

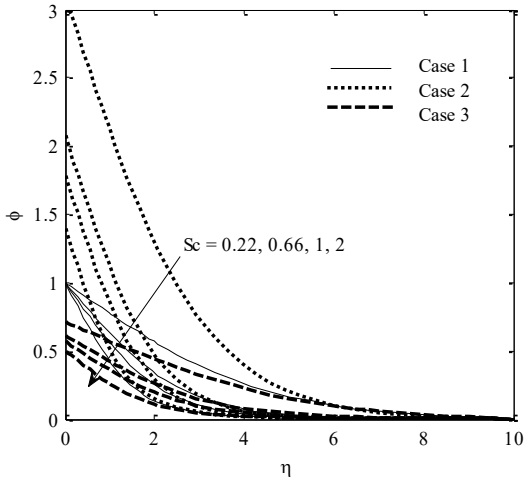

Fig. 6 (c) Concentration profile Effected by Sc

IV. CONCLUSION

In this study, we have examined the steady incompressible free convective fluid flow across an isothermal sphere. The results, which were obtained by numerical approaches, are displayed in graphs. The results demonstrate that the relevant parameters have a significant impact on the velocity, temperature, and concentration profiles. For constant wall temperature and concentration (case 3), the velocity, temperature, and concentration profiles are slightly higher than those in the other two scenarios. These results allow for the following deductions to be made:

- In all three scenarios, an increase in permeability strength causes temperature and concentration to drop while velocity increases concurrently.
- When the combined impacts of the Soret and Dufour numbers are examined, it can be seen that while the Dufour number has the opposite effect, an increase in the Soret number improves the concentration profile while decreasing temperature and velocity.

REFERENCES

[1] Miyatake, O. and T. Fuzii (1972). Free convection heat transfer between vertical parallel plates–one plate isothermally heated and the other thermally insulated, *Heat Transfer: Japanese Research*, 3, 30–38.

[2] Merkin, J.H. and M. A. Chaudhary (1994). Free-convection boundary layers on vertical surfaces driven by an exothermic surface reaction, *Quarterly Journal of Mechanics and Applied Mathematics*, 47, 405–428.

[3] Paul, T., B. K. Jha and A. K. Singh (1996). Transient free convective flow in a vertical channel with constant temperature and constant heat flux, *Heat and Mass Transfer*, 32 (1/2), 61–63.

[4] Kawala, A. M. and S. N. Odda (2013). Numerical Investigation of Unsteady Free Convection on a Vertical Cylinder with Variable Heat and Mass Flux in the Presence of Chemically Reactive Species, *Advances in Pure Mathematics*, 3, 183-189.

[5] Chiang, T., A. Ossin and C. L. Tien (1964). Laminar free convection from a sphere. *ASME Journal of Heat Transfer*, 86, 537–542.

[6] Huang, M. J. and C. K. Chen (1987). Laminar free convection from a sphere with blowing and suction, *ASME Journal of Heat Transfer*, 109, 529–532.

[7] Molla, M. M., M. A. Hossain and R. S. R. Gorla (2004). Conjugate effect heat and mass transfer in natural convection flow from an isothermal sphere with chemical reaction. *International Journal of Fluid Mechanics and Research*, 31, 319–331.

[8] Molla, M. M., U. K. Glasgow, M. A. Hossain and M. A. Taher (2006). Magnetohydrodynamic natural convection flow on a sphere with uniform heat flux in presence of heat generation, *Acta Mechanica*, 186, 75–86.

[9] Molla, M. M., M. A. Hossain and S. Siddiqa (2006). Radiation effect on free convection laminar flow from an isothermal sphere, *Chemical Engineering Communication*, 198, 1483-1496.

[10] Nazar, R., N. Amin, T. Grosan and I. M. Pop (2002). Free convection boundary layer on an isothermal sphere in a micropolar fluid, *International Communications in Heat and Mass Transfer*, 29, 377-386, 2002.

[11] Nazar, R., N. Amin, T. Grosan and I. M. Pop (2002). Free convection boundary layer on a sphere with constant surface heat flux in a micropolar fluid, *International Communications in Heat and Mass Transfer*, 29, 1129-1138.

[12] Akhter, T. and M. A. Alim (2008). Effects of radiation on natural convection flow around a sphere with uniform surface heat flux, *Journal of Mechanical Engineering*, 39(1), 50-56.

[13] Chamkha, A., R. S. R. Gorla and K. Ghodeswar (2011). Non-similar solution for natural convective boundary layer flow over a sphere embedded in a porous medium saturated with a nanofluid, *Transport Porous Media*, 86, 13–22.

[14] Gaffar, S. A., V. R. Prasad, E. K. Reddy and O. A. Bég (2014). Free convection flow and heat transfer of non-newtonian tangent hyperbolic fluid from an isothermal sphere with partial slip, *Arabian Journal for Science and Engineering*, 39, 8157–8174.

[15] Gaffar, S. A., V. R. Prasad, E. K. Reddy and O. A. Bég (2015). Thermal radiation and heat generation/absorption effects on viscoelastic double-diffusive convection from an isothermal sphere in porous media, *Ain Shams Engineering Journal*, 6, 1009–1030.

[16] Alkasasbeh, H. T., Mohd Zuki Salleh, R. M. Tahar, R. Mohd Nazar and I. M. Pop (2015). Effect of radiation and magnetohydrodynamic free convection boundary layer flow on a solid sphere with convective boundary conditions, *Walailak Journal of Science and Technology*, 12(9), 849-861.

[17] Dursunkaya, Z. and W. M. Worek (1992). Diffusion-thermo and thermal-diffusion effects in transient and steady natural convection from vertical surface, *International Journal of Heat and Mass Transfer*, 35, 2060–2067.

[18] Pandya, N. and A. K. Shukla (2014). Soret-Dufour and radiation effect on unsteady MHD flow over an inclined porous plate embedded in porous medium with viscous dissipation. *International journal of advances in applied mathematics and mechanics*, 2(1), 107–119.

[19] Bhargava, R., R. Sharma and O. A. Bég (2009). Oscillatory chemically-reacting MHD free convection heat and mass transfer in a porous medium with Soret and Dufour effects: finite element modeling, *International Journal of Applied Mathematics and Mechanics*, 5 (6), 15–37.

[20] Cheng, C.Y. (2009). Soret and Dufour effects on natural convection heat and mass transfer from a vertical cone in a porous medium, *International Communications in Heat and Mass Transfer*, 36(10), 1020–1024.

[21] EL-Kabeir, S. M. M., A. J. Chamkha, A. M. Rashad, H. F. Al-Mudhaf (2010). Soret and Dufour effects on heat

and mass transfer by nondarcy natural convection from a permeable sphere embedded in a high porosity medium with chemically-reactive species, *International Journal of Energy & Technology*, 2 (18), 1–10.

[22] Bég, A., V. R. Prasad, B. Vasu, N. B. Reddy, Q. Li and R. Bhargava (2011). Free convection heat and mass transfer from an isothermal sphere to a micropolar regime with Soret/Dufour effects, *International Journal of Heat and Mass Transfer*, 54, 9–18.

[23] Srinivasacharya, D. and U. Mendu (2015). Mixed convection in MHD doubly stratified micropolar fluid, *Journal of the Brazilian Society of Mechanical Sciences and Engineering*, 37, 431–440.

[24] Srinivasacharya, D. and O. Surender (2015). Effect of double stratification on mixed convection boundary layer flow of a nanofluid past a vertical plate in a porous medium, *Applied Nanoscience*, 5, 29–38.

[25] Swarnalathamma, B. V. (2018). Heat and Mass transfer on MHD flow of Nanofluid with thermal slip effects, *International Journal of Applied Engineering Research*, 13(18), 13705-13726.

[26] Rao A. S., Sainath S., Rajendra P. and Ramu G. (2019). Mathematical Modelling of Hydromagnetic Casson non-Newtonian Nanofluid Convection Slip Flow from an Isothermal Sphere, *De Gruyter's Journal of Nonlinear Engineering vol.8 issue(1)*.

[27] Sedki A. M. (2022). Effect of thermal radiation and chemical reaction on MHD mixed convective heat and mass transfer in Nanofluid flow due to nonlinear stretching *surface* through porous medium, *Elsevier Results in Materials*,16, 100334.

[28] Krishna M. V., Kamboji J. and Chamkha A. J. (2020) Heat and mass transfer on MHD flow of Second-grade fluid through porous medium over a semi-infinite vertical stretching sheet, *Journal of Porous Media*, 23(8), 751–765.

[29] Pal D., Dasb B. C. and Vajraveluc K. (2022). Magneto-Soret-Dufour thermo-radiative double-diffusive convection heat and mass transfer of a micropolar fluid in a porous medium with Ohmic dissipation and variable thermal conductivity, *Elsevier Propulsion and Power Research*,11(1), 154-170.

[30] Abbas A., Sarris I. E., Ashraf M., Ghachem K. , Hnaien N. and Alshammari B. M. (2023) The effects of reduced gravity and radiative heat transfer on the magnetohydrodynamic (MHD) flow past a non-rotating stationary sphere surrounded by a porous medium. *Mdpi symmetry*, 15 (4).

[31] Keshavarzian, B., & Sayehvand, H. O. (2023). Validation of the local thermal equilibrium assumption for free convection boundary layer flow over a horizontal cylinder embedded in an infinite saturated porous medium. *Results in Physics*, *44*, 106112.

[32] Hamida, M. B. B. (2024). numerical study using hybrid nanofluid to control heat and mass transfer in a porous media. *thermal science*, 28(1B), 703-715.

[33] Francis, P., Sambath, P., Fernandez-Gamiz, U., Noeiaghdam, S., & Dinarvand, S. (2024). Computational analysis of bio-convective eyring-powell nanofluid flow with magneto-hydrodynamic effects over an isothermal cone surface with convective boundary condition. *Heliyon*, 10(3).

[34] Khan, W., Saidani, T., Smarandache, F., Khan, M. S., Ayed, H., & Abdou, M. M. M. (2024). Two-dimensional steady squeezing flow over a vertical porous channel with free convective heat/mass transfer and invariable suction. *Case Studies in Thermal Engineering*, *60*, 104800.

